The Separation of Two Different Sized Particles in an Evaporating Droplet

Nicole Raley Devlin, Katherine Loehr, and Michael T. Harris
Dept. of Chemical Engineering, Purdue University, West Lafayette, IN

DOI 10.1002/aic.14977
Published online August 22, 2015 in Wiley Online Library (wileyonlinelibrary.com)

The separation of two different sized particles during evaporation of a dilute droplet is examined both computationally and experimentally. A transport model of the evaporating droplet system was solved using the finite element method to determine the fluid velocity, pressure, vapor concentration surrounding the droplet, temperature, and both particle concentrations. Experimentally, 1 μm and 3 μm polystyrene particles were used during the evaporation of a sessile water droplet. It was determined that to accurately model particle deposition, thermal effects need to be considered. The Marangoni currents in evaporating droplets keep particles suspended in the droplet until the end of the evaporation. Previous models of particle deposition during droplet evaporation have rapid accumulation of particles at the contact line. Our experiments and the experiments of others demonstrate that this is not accurate physically. In addition, to model the separation of two different sized particles the consideration of thermal effects is essential. © 2015 American Institute of Chemical Engineers *AIChE J*, 61: 3547–3556, 2015
Keywords: evaporation, particle technology, fluid mechanics, transport

Introduction

Particle deposition from droplet evaporation has been studied extensively in the past few decades.[1–4] When there are particles in the drying droplet (such as when coffee drys on a counter-top), the drying process has a pinned contact line for the majority of evaporation. This was shown by Pariss and Allain in 1996 by comparing two models (one for pinned contact line and one for constant contact angle) to experimental results.[5] Only at the end, when the contact angle becomes very small, does the contact line detach and recede inward. The radial flow necessary to replenish fluid at the contact line causes the coffee ring effect. Particles within the fluid are pushed radially outward with the flow and gather at the contact line.

Computationally, it has been shown that the deposition profile depends on both mass transfer of particles in the bulk fluid (dimensionless Péclet number, $Pe=l_c v/D_p$ where l_c is the characteristic length, v_c is the characteristic velocity, and D_p is the particle diffusivity) and on the deposition rate of particles on the substrate (dimensionless Damköhler number, $Da=k_d l_c/D_p$ where k_d is the particle deposition rate constant onto the substrate).[6]

In 2005, Yuri Popov examined droplet evaporation with particles both analytically and numerically.[7] With an assumption of a thin droplet, low Reynolds number, and dilute particle concentration, Popov showed that particle accumulation at the contact line is constrained geometrically. Small droplet contact angles impede particle rings from accumulating in the z-direction (height) and force the ring to grow radially inward (thicker).

Recently, the effects of Marangoni currents on droplet evaporation has been studied quite a bit.[4,8] Marangoni flow causes circular currents in the evaporating droplet. The evaporative cooling that happens on the droplet surface leads to a temperature gradient on the liquid–gas interface. Consequentially, the surface tension is affected by this temperature gradient (higher temperatures lead to lower surface tension). Fluid will flow from an area of low surface tension to an area of high surface tension. As the drop evaporates, the surface is cooled causing a temperature gradient.

The Marangoni currents in an evaporating drop have been observed experimentally using coherence tomography and out-of-focus microscopy.[9–11] An evaporating droplet without particles was modeled by Girard et al. in 2006 using the finite element method to show the Marangoni currents during evaporation computationally.[12] Girard et al. later determined (2008) that the total drop evaporation rate is not significantly affected by Marangoni flow currents for a droplet on a heated substrate.[8] Around the same time, Hu and Larson used two approaches to study Maragoni currents in an evaporating droplet. The first approach was using the lubrication theory approximation to analytically examine the evaporation of a sessile droplet with Marangoni effects and second approach was using the finite element method to computationally analyze the problem. Their two solutions were in good agreement with each other and both showed circulation eddies driven by the surface tension gradient.[4] More recently, Bhardwaj et al modeled a nanoliter sized droplet with particles and Marangoni effects. Bhadarwaj showed that the conductivity of the solid substrate compared to the conductivity of the liquid determines the direction that the Marangoni eddy flows.[13] This

Correspondence concerning this article should be addressed to M. T. Harris at mtharris@purdue.edu.

effect was also examined theoretically by Ristenpart et al.[14] and with experiments and a mathematical model by Dunn et al.[15]

There has been speculation as to whether a nonheated, water droplet without surfactants has Marangoni currents in the droplet. To examine this question, Xu and Luo used fluorescent nanoparticles to analyze an evaporating water droplet with a radius of 2 mm on a glass substrate.[16] Their research showed that the nanoparticles travel to the edge of the droplet and then travel back toward the center. This particle pattern indicates that circulating Marangoni currents are present in an evaporating water droplet. In addition, our experimental observations of particles in evaporating droplets from this research show circulating Marangoni currents in unheated evaporating water droplets.

Separately, research was conducted to explore the phenomena particle manipulation during deposition via droplet evaporation. The deposition of particles in interesting patterns has been observed for quite some time. In 1992, Denkov et al. created ordered monolayers of polystyrene particles using an evaporating drop inside a Teflon ring.[17,18] The aqueous drop was 20 μL, larger than most drops in more recent investigations. The particles deposited were 1.7 μm diameter polystyrene particles with an initial concentration of 1 wt %. Denkov et al. determined that the particle ordering occurred when the water layer was thinner than the particle size. Additionally, the droplet evaporation rate and the droplet shape significantly contributed to the final pattern of particles.

In 1995, Adachi et al. observed striped patterns at the edge of an evaporating droplet using 144 nm polystyrene particles in water and a borosilicate glass substrate.[19] Adachi et al. found that the stripe pattern is highly dependent on the particle volume fraction in the droplet. It was also determined that as the drop evaporates, its contact line oscillates, which could contribute to the striped particle pattern.

Following Adachi et al.'s work, Shmuylovich et al. experimentally observed a stick-slip behavior at the contact line of an evaporating droplet.[20] Using 0.88 μm latex particles in a water solution, Shmuylovich et al. deposited drops between 1 mm and 15 mm diameter on a glass substrate. It was observed that at the edge of the droplet, particles accumulate and then the contact line moves slightly inward slipping and then it stays at that new position to allow more particles to accumulate sticking. In this fashion, concentric rings are made during the droplet evaporation process.

The previously discussed work examined only a single particle size, however, some studies examine multiple sized particles. In 2009, Erb et al. showed that using an electric field, particles of multiple sizes can be manipulated into self-assembled shapes. In this study, 1 μm nonmagnetic particles and 2.7 μm paramagnetic particles were dispersed in a ferromagnetic fluid. A constant electric field was applied and a phase diagram depicting different particle assemblies was generated. In the phase diagram, random distribution, poles (small particles aggregated on each side of a large particle), and rings (small particles surrounding a large particle) are plotted as a function of the ferrofluid concentration and the electric field strength.[21]

Han et al. also showed that particles of different sizes can be manipulated into different patterns. In this study, instead of an electric field, a confined geometry using a cylindrical lens and heated silicon substrate ($T = 80$°C) were used. Polystyrene particles of 50 nm and 500 nm self-assembled into lines of each size using this setup.[22]

Dip coating has also been used to create highly ordered nanopatterns. Huang et al. used dip coating to self assemble 100 nm gold nanoparticles and 50 nm silver nanoparticles on to a Si/SiO_2 substrate. The resulting substrates had highly ordered, dense line patterns made from the nanoparticles.[23]

In the past few years, some experimental studies were published on using droplet evaporation to naturally separate particles. During the evaporation process, particles of different sizes were separated into different rings. The smaller particle size accumulated on the outer ring and the larger particle size accumulated on the inner ring. In 2007, Jung et al. separated 1 μm and 6 μm polystyrene particles using a nonuniform electric field to induce dielectrophoresis in the droplet.[24] A follow up study by Jung et al. in 2009 used particle velocimetry to track particle movement during the separation of 5 μm and 0.5 μm polystyrene particles.[25] Following their work, in 2011 Wong et al. showed the separation of three different sized particles: 40 nm, 1 μm and 2 μm.[26] Wong et al. related the separation distance to the difference in particle size and determined a maximum particle concentration for which this separation phenomenon is observed.

The work presented here explores the contribution of Marangoni currents on the particle separation process that naturally occurs during droplet evaporation. Particle separation on a small-scale, such as in droplet evaporation, affects technology such as bioassays and lab-on-a-chip devices. It has potential in virus detection and separation abilities and is thus a worthy problem to study.

Methods

Inside the droplet, the transport model solves for the radial velocity u, the axial velocity v, the pressure p, the temperature T, and two particle concentrations c_{p1} and c_{p2}. Equations 1 and 2 solve for the fluid profiles (u, v, and p)

$$ReCa\frac{\partial \mathbf{v}}{\partial t}+ReCa\mathbf{v}\cdot\nabla\mathbf{v}=Ca\nabla\cdot\mathbf{T} \tag{1}$$

$$\mathbf{T}=-p+[\nabla\mathbf{v}+(\nabla\mathbf{v})^T]$$

$$\frac{\partial \rho}{\partial t}+\nabla\cdot(\rho\mathbf{v})=0 \tag{2}$$

where the Reynolds number is $Re=\rho v_c l_c/\mu$, the Capillary number is $Ca=\mu v_c/\gamma$, and $\mathbf{v}$ is the velocity vector with both a radial component u and an axial component v. Within each dimensionless number μ is the viscosity, ρ is the density, v_c is the characteristic velocity as defined in Table 1.

The temperature inside the droplet (T) is governed by Eq. 3

$$\hat{P}e\left[\frac{\partial T}{\partial t}+\mathbf{v}\cdot\nabla T\right]=\nabla^2 T \tag{3}$$

where the Péclet number is $\hat{P}e=v_c l_c/\alpha$ and the thermal diffusivity $\alpha=k/\rho\hat{C}_p$ with k as the thermal conductivity and $\hat{C}_p$ as the specific heat capacity. Finally, the particle concentrations c_{p1} and c_{p2} inside the droplet are governed by Eqs. 4 and 5, respectively. The simulation of two particle sizes in an evaporating droplet is a novel addition to this problem, previous computational studies only examined one particle size.[13,32,33] An assumption in this model is that the particles are very dilute and do not interact with each other

$$Pe_1\left(\frac{\partial c_{p1}}{\partial t}+\mathbf{v}\cdot\nabla c_{p1}\right)=\nabla^2 c_{p1} \tag{4}$$

Table 1. Simulation Parameters

Variable	Equation/Definition	Value	Units
l_c	drop radius	1×10^{-3}	m
c_v	saturation concentration[13]	2.32×10^{-2}	kg/m^3
D	Diffusivity of water in air[27]	26.1×10^{-5}	m^2/s
v_c	$Dc_v/\rho l_c$	6.0552×10^{-6}	m/s
k	thermal conductivity[28]	0.58	W/m K
C_p	specific heat capacity[29]	4.181	kJ/kg K
α	$k/\rho C_p$	1.387×10^{-7}	m^2/s
$\hat{P}e$	$v_c l_c/\alpha$	4.36×10^{-2}	–
μ	viscosity[30]	8.9×10^{-4}	Pa s
γ	surface tension	varies	N/m
ρ	density of fluid	varies	kg/m^3
Ca	$\mu v_c/\gamma$	7.402×10^{-8}	–
Re	$\rho v_c l_c/\mu$	6.8×10^{-3}	–
H_v	latent heat of vaporization[31]	2260	kJ/kg
k_B	Boltzmann constant	1.38×10^{-23}	m^{2}kg/s^2 K
Pe	$v_c l_c/D_p$	varies	–
Da	kl_c/D_p	varies	–
D_p	particle diffusivity	varies	–

$$Pe_2\left(\frac{\partial c_{p2}}{\partial t}+\mathbf{v}\cdot\nabla c_{p2}\right)=\nabla^2 c_{p2} \tag{5}$$

where the Péclet number is $Pe=v_c l_c/D_p$, D_p is the particle diffusivity, c_{p1} is the first particle concentration and c_{p2} is the second particle concentration. The specific quantities for these values are listed in Table 1. The dimensionless numbers will vary according to particle size as seen in Eqs. 6–8

$$Pe_i=\frac{l_c v_c}{D_{pi}} \tag{6}$$

$$Da_i=\frac{k_i l_c}{D_{pi}} \tag{7}$$

$$D_{pi}=\frac{k_B T}{6\pi\mu a_i} \tag{8}$$

In the above equations, D_p is the particle diffusivity, k_B is the Boltzmann constant, T is temperature, k is the particle adhesion constant to the surface, a is particle radius, and $i=1$, 2 is the particle number. As the particle radius increases, the Péclet number and Damköhler number increase in a linear fashion. The Péclet number represents the ratio of convective forces to diffusive forces. For a larger particle size the convective forces will increase, which pushes the larger particles toward the contact line at a faster rate than the smaller particles. This is contrary to what is observed experimentally where the smaller particles gather at the outer edge of the droplet.

Outside of the droplet, the concentration of vapor in the gas, c, is modeled using the Laplace equation 9. This model accounts for simple diffusion of the vapor into the surrounding air. It assumes that the gas surrounding the droplet is not moving and that the drop evaporates slowly. Quasi steady-state $\left(\frac{\partial c}{\partial t}=0\right)$ is assumed because of the slow evaporation and it is also assumed that the concentration profile in the gas phase is established very fast

$$\nabla^2 c=0 \tag{9}$$

The domain for which the vapor concentration is modeled extends from the drop surface to a distance of $20R$, which is 20 times the radius of the drop in both the r and z direction. This domain was chosen based on the research of Hu and Larson.[34]

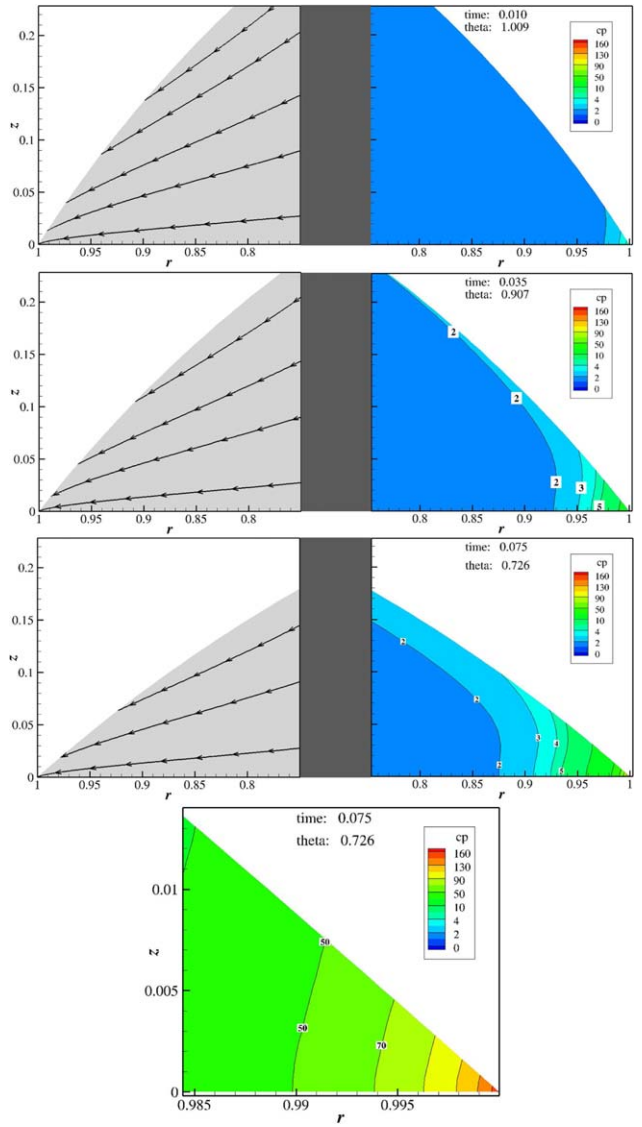

Figure 1. In an isothermal droplet, the particles accumulate rapidly at the contact line.

In the first three image figures the streamlines in the droplet are shown on the left and the particle concentration on the right at times 0.01, 0.035, and 0.075. The last image is a zoomed in picture of time 0.075 to show the high particle concentration at the contact line. [Color figure can be viewed in the online issue, which is available at wileyonlinelibrary.com.]

Boundary and initial conditions

Liquid–Gas Interface. The liquid–gas interface moves as the droplet evaporates and its location needs to be determined. Equation 10 is used to determine the location of the liquid–gas interface as the drop evaporates

$$\mathbf{n_s}\cdot(\mathbf{v}-\mathbf{v_s})=-\mathbf{n_s}\cdot\nabla c \tag{10}$$

where $\mathbf{n_s}$ is the surface normal and $\mathbf{v_s}$ is the velocity at the surface. Equation 10 (the kinematic boundary condition) balances the movement of the interface (left-hand side) with the amount of liquid that is exiting the drop from evaporation (the right-hand side).

To prevent particles from evaporating with the droplet, Eq. 11 is used as a boundary condition for each particle equation

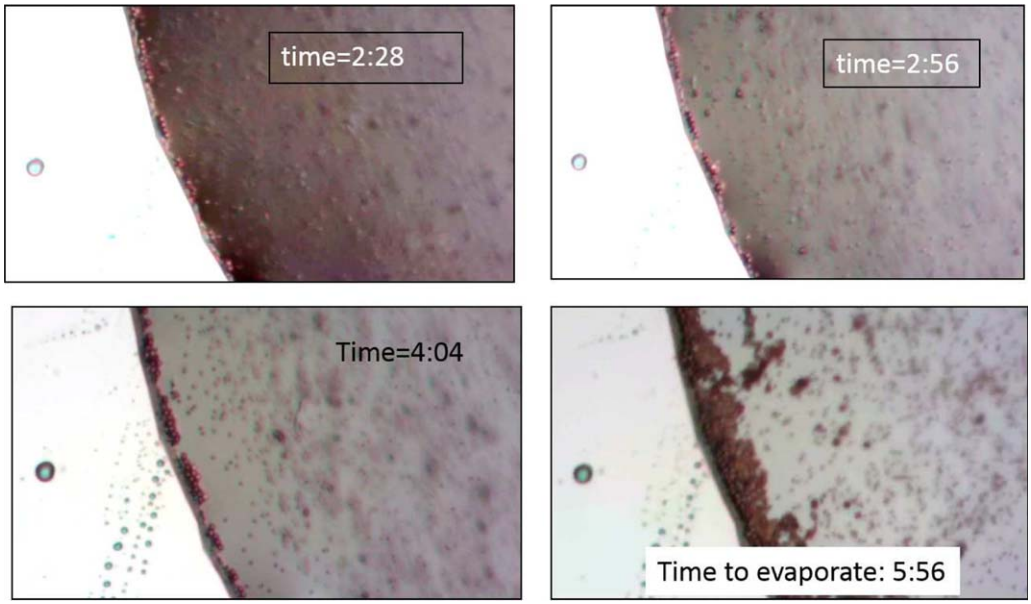

Figure 2. The contact line of an aqueous 2 μL droplet during evaporation.

The particles accumulate at the contact line primarily at the end of the evaporation. At time = 4:04 min, most of the particles are still in solution. Only at the end of the evaporation is the maximum packing concentration of particles reached. [Color figure can be viewed in the online issue, which is available at wileyonlinelibrary.com.]

$$\mathbf{n_s} \cdot \nabla c_{pi} = Pe_i \mathbf{n_s} \cdot c_{pi}(\mathbf{v} - \mathbf{v_s}) \tag{11}$$

Finally, to account for the evaporative cooling that occurs on the liquid–gas interface, Eq. 12 is used as a boundary condition for the thermal equation.

$$JH_v = -k\mathbf{n_s} \cdot \nabla T \tag{12}$$

where J is the dimensional flux of vapor out of the droplet, H_v is the latent heat of vaporization, k is the thermal conductivity, and T is temperature.

Liquid–Solid Interface. At the substrate surface ($z = 0$, $r \leq R$) Eq. 13 is applied to the governing equations

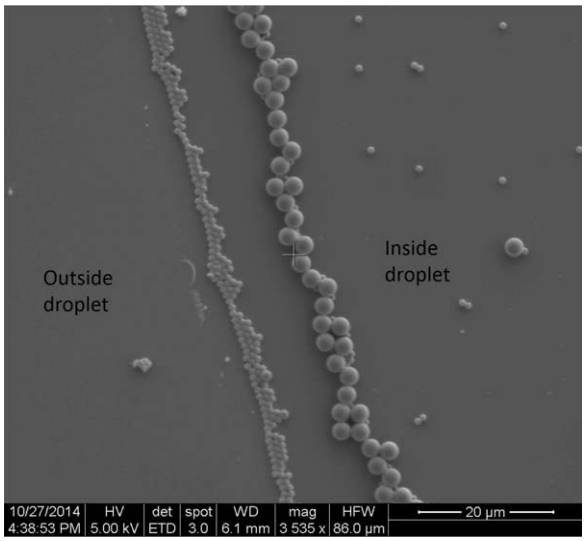

Figure 3. One and three micrometer sized particles aligned into rings during the droplet evaporation.

The droplet was 2 μL and the initial particle concentration was 0.025 wt % with equal parts of each particle size. The evaporation occurred on an unheated smooth silicon substrate in a zero humidity environment.

$$\begin{aligned} u &= 0 \\ v &= 0 \\ T &= T_s \\ -\mathbf{n_s} \cdot \nabla c_{p1} &= Da_1 cp_1 \\ -\mathbf{n_s} \cdot \nabla c_{p2} &= Da_2 cp_2 \end{aligned} \tag{13}$$

where T_s is the substrate temperature which is constant for the entire evaporation. This constant substrate temperature boundary condition assumes that the substrate is a good conductor.

Axis of Symmetry Boundary. The final boundary condition inside the droplet is the axis of symmetry ($r = 0$, $0 \leq z \leq z_{\max}(t)$). At the $r = 0$ boundary, Eq. 14 is used as boundary conditions to keep the drop symmetric.

$$\begin{aligned} \mathbf{n} \cdot \mathbf{v} &= 0 \\ \mathbf{n} \cdot \mathbf{T} \cdot \mathbf{t} &= 0 \\ \mathbf{n} \cdot \nabla T &= 0 \\ \mathbf{n} \cdot \nabla c_{p1} &= 0 \\ \mathbf{n} \cdot \nabla c_{p2} &= 0 \end{aligned} \tag{14}$$

where $\mathbf{t}$ is the tangent to the boundary. Note the distinction between $\mathbf{T}$ the stress tensor used in the momentum equation and T the temperature used in the thermal equation.

Initial Conditions. The initial conditions are in listed in Eq. 15

$$\begin{aligned} v(r, z, t_0) &= 0 \\ u(r, z, t_0) &= 0 \\ p(r, z, t_0) &= \frac{2}{Ca} \\ T(r, z > 0, t_0) &= T_\infty \\ T(r, 0, t) &= T_s \\ c_{p1}(r, z, t_0) &= 1 \end{aligned}$$

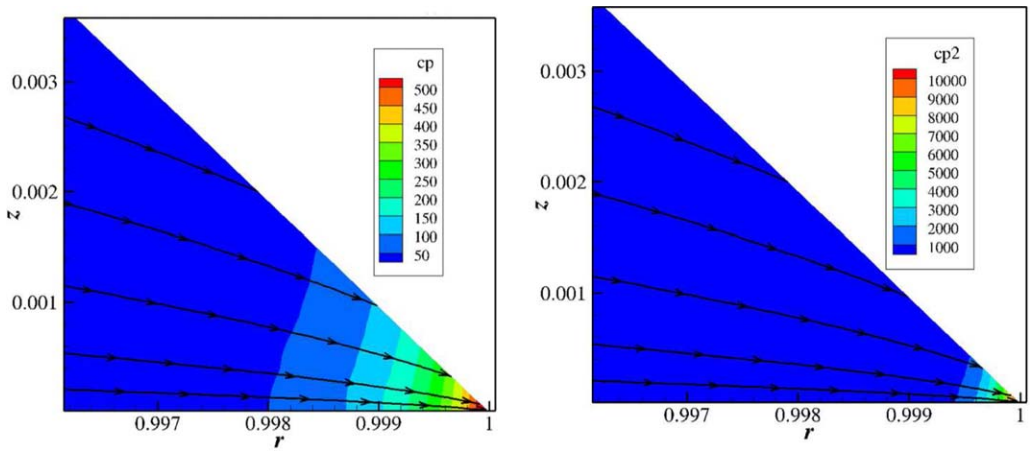

Figure 4. The build up of particles at the edge of an evaporating droplet for both 1 μm sized particles (left) and 3 μm sized particles (right) after the evaporation is only 4% completed.

The larger particles build up much faster than the smaller particles at the edge, which does not match with experimental results. With the rapid buildup of large particles early on in the evaporation, smaller particles are unable to travel around the larger particles to form the outer ring that is seen in experiments. [Color figure can be viewed in the online issue, which is available at wileyonlinelibrary.com.]

$$c_{p2}(r,z,t_0)=1 \tag{15}$$

The initial pressure, p, inside of the drop is obtained from the Young–Laplace equation for a hemispherical drop, T_∞ is the ambient temperature, and t_0 is the starting time.

The Vapor Domain. Outside of the drop, the following boundary conditions are used to solve the Laplace equation

$$\begin{aligned} c=c_{\text{vap}}=1 \quad &\text{at} \quad \text{the drop interface} \\ c=c_\infty \quad &\text{at} \quad r=20R \\ \mathbf{n}\cdot\nabla c=0 \quad &\text{at} \quad r=0 \text{ and } z=0 \end{aligned} \tag{16}$$

where $c_\infty=Hc_{\text{vap}}$ and H is the humidity. The initial concentration of vapor in the gas phase is given by Eq. 17

$$c(r,z,t_0)=\frac{1-H}{\sqrt{r^2+z^2}}+H \tag{17}$$

Parameters and code validation

Table 1 lists the simulation parameters for the work presented. The simulation variables are calculated for a water droplet with a 1 mm radius. Although the temperature is changing, it is assumed that saturation concentration, latent heat of vaporization, viscosity, and thermal conductivity are constant.

Validation of the fluid and particle transport models are presented in the Appendix. The evaporative flux computed by the code is in excellent agreement with the results of Deegan.[2] The mass balance calculations confirmed the accuracy of the particle transport model.

Experimental methods

To compliment the computational transport model, experiments were performed with aqueous 1 μm and 3 μm

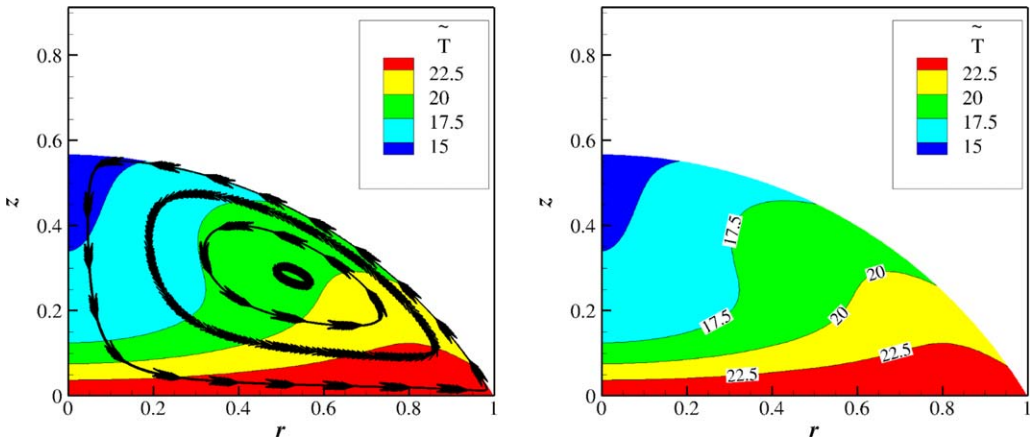

Figure 5. Nonisothermal simulation showing Marangoni currents in the evaporating droplet.

The substrate temperature is unheated (fixed to 25.1°C), the humidity is zero, the Capillary number is $Ca=8.4\times10^{-7}$, the Reynolds number is $Re=6.8\times10^{-3}$, and the thermal Péclet number $\hat{Pe}=4.36\times10^{-2}$. The evaporative cooling causes the cooling temperature dip seen in the center of the drop. Note that the temperature shown ($\tilde{T}$) is a dimensional temperature in °C. [Color figure can be viewed in the online issue, which is available at wileyonlinelibrary.com.]

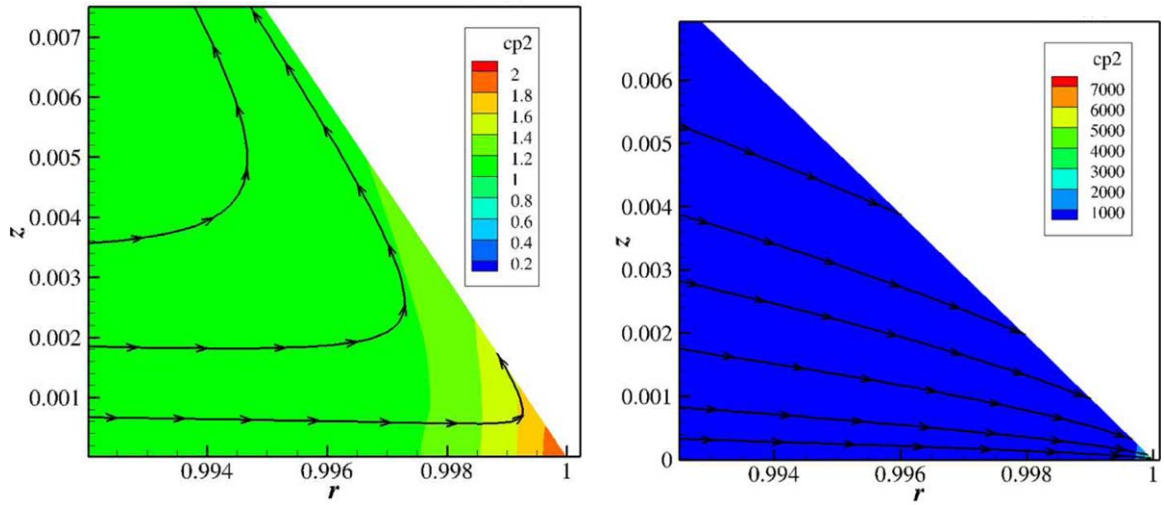

Figure 6. This image shows the build up of 3 μm sized particles at the contact line of an evaporating droplet.

On the left thermal variation is considered and the streamlines circulate due to Marangoni currents. On the right the droplet is isothermal and the particles rapidly build up on the contact line. The isothermal model does not match experimental results, but the model that considers thermal variation does match experimental results. [Color figure can be viewed in the online issue, which is available at wileyonlinelibrary.com.]

polystyrene particles which were generously provided by PolySciences Inc. The particle solutions were diluted to the desired droplet concentration using millipore water. The evaporation substrate was silicon and evaporations took place on a vibration minimizing table and in a humidity controlled box which also minimized air currents (necessary for the quasi-steady state assumption used to model the vapor concentration).

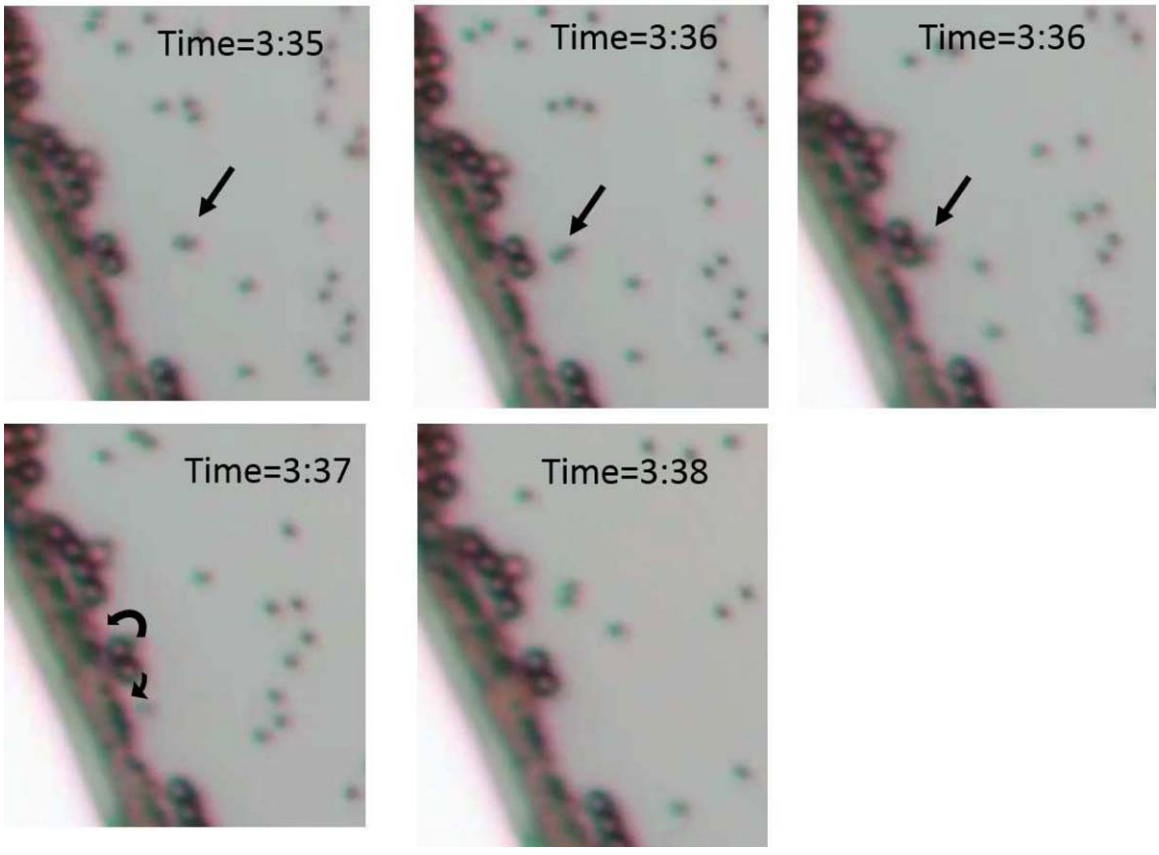

Figure 7. Images from a video of particles depositing on the contact line of an aqueous evaporating droplet.

The original droplet volume was 2 μL and the original particle concentration was 0.025 wt %. Each image is a different time progressing from left to right and top to bottom. There are two different sized particles 1 μm and 3 μm. The arrows point to two 1 μm particles as they are depositing at the contact line. At time 3:37 min, the two 1 μm particles travel around the larger 3 μm particles and deposit closer to the edge of the droplet. A Supporting Information video of this evaporation can be provided upon request. [Color figure can be viewed in the online issue, which is available at wileyonlinelibrary.com.]

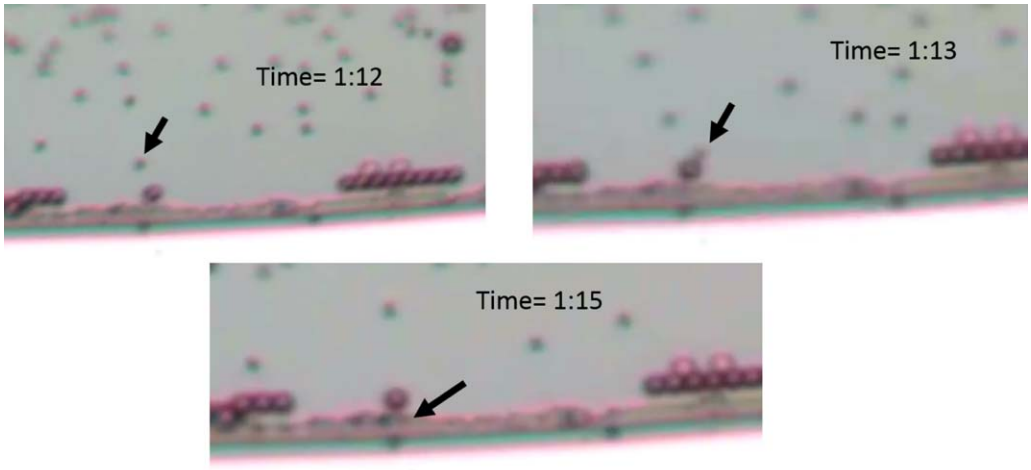

Figure 8. Images from a video of particles depositing on the contact line of an aqueous evaporating droplet.

The original droplet volume was 2 μL and the original particle concentration was 0.025 wt %. Each image is a different time progressing from left to right and top to bottom. There are two different sized particles 1 μm and 3 μm. The arrows point to a 1 μm particle as as it deposits at the contact line. At time 1:12 min, the 1 μm particle approaches the larger 3 μm particles, at 1:13 the 1 μm particle touches or comes within close proximity of the 3 μm particle and then travels around it. Finally, at 1:15 the 1 μm particle deposits at the edge of the droplet, closer to the contact line than the 3 μm particle. A Supporting Information video of this evaporation can be provided upon request. [Color figure can be viewed in the online issue, which is available at wileyonlinelibrary.com.]

Evaporations were imaged in three different ways. The videos were taken with tablet PC with a 5.0 mega pixel camera attached to a microscope. After the evaporation was finished the deposited particles were coated with 10 Å of platinum metal with a Cressington sputter coater and imaged using a FEI Nova Nano scanning electron microscope or were imaged without a metal coating using a Bruker Multi Mode atomic force microscope.

Results and Discussion

Without Marangoni currents, particles in an evaporating droplet accumulate rapidly at the droplet contact line. Figure 1 shows the build up of particles over time in an evaporating isothermal droplet. The evaporation shown is a water droplet with a radius of 1 mm and particles with a diameter of 100 nm. The Péclet number is of $\mathcal{O}(10^3)$. This flow is highly convective and the particles accumulate very rapidly at the surface. Figure 1 shows the accumulation of particles with a Péclet number of 10. Note that a lower Péclet number is used to reduce the computational time for this simulation, but even with the reduced *Pe* the particles accumulate rapidly at the contact line.

In contrast, during our experiments, the particles did not deposit until the end of the evaporation. Figure 2 shows the buildup of particles at the contact line of an aqueous evaporating 2 μL droplet. This observation was recently made in another experimental study as well by Parsa et al.[35] For these reasons, the current computational method of determining particle accumulation and deposition onto a substrate during droplet evaporation is not sufficient.

In addition, the current method of particle accumulation and deposition does not match experimental results when there are two different particle sizes in the droplet. When there are two different sized particles in a droplet, the particles can separate during the evaporation process and form different rings for each particle size with the smaller particle on the outer edge of the droplet. Figure 3 shows the separate rings formed during our experiments on the evaporation of a 2 μL aqueous drop with 0.025 wt % of 1 μm and 3 μm polystyrene spheres. The

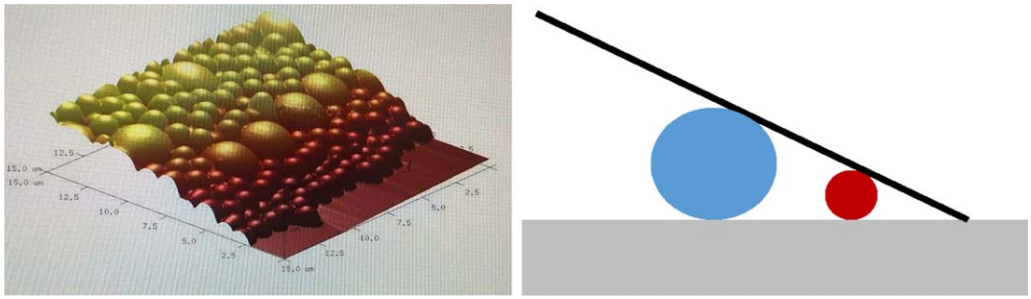

Figure 9. On the left is an Atomic Force Microscopy (AFM) image of the ring formed during the evaporation of 1 μm and 3 μm polystyrene spheres in an aqueous solution on a glass substrate.

The drop solution contained 0.165 wt % particles. The 1 μm particles are accumulated at the edge because the larger 3 μm particles are constrained geometrically from approaching the outer edge of the contact line. This was consistent around the entire ring of the droplet. The figure on the right shows a sketch of how the larger particles are geometrically constrained by the contact angle. [Color figure can be viewed in the online issue, which is available at wileyonlinelibrary.com.]

particles separated during the evaporation process with the smaller (1 μm) particles on the outer edge of the droplet and the larger (3 μm) particles on the inner part of the droplet, which is consistent with literature.

Figure 4 shows the accumulation of two different sized particles in a simulation that uses Eqs. 4 and 5 and **no** thermal variation to model particle concentration. The 3 μm sized particles accumulate much more rapidly at the contact line than the 1 μm sized particles. As seen in Figure 3 and in experiments conducted by other researchers,[26] this computational result shows higher concentration of the larger particles at the outer edge of the droplet and does **not** match experimental results. Thus, a new model to track particle accumulation is needed.

When thermal variation in the droplet is considered, the streamlines in the evaporating droplet differ significantly due to Marangoni currents (shown in Figure 5). As the particles follow these streamlines, the particle deposition also varies significantly. Looking at the particle accumulation with and without thermal effects considered, we can see that when thermal effects are accounted for the model matches experiments (Figure 6). The Marangoni currents keep particles suspended in the droplet for the majority of the evaporation. It is only at the end of the evaporation, when the drop is very thin, that the particles accumulate rapidly at the contact line.

Finally, the deposition of individual particles during an evaporation was filmed. Figures 7 and 8 show how smaller 1 μm sized particles will travel around the larger 3 μm particles, which are stopped from their geometric constraints. Figure 9 demonstrates the geometric constraints of the larger particles when approaching the contact line. Corresponding this result to the computational results, it is not necessary for the smaller particles to deposit first in the model. Instead, it is only necessary for there to be a concentration lower than the maximum packing concentration so that the smaller particles can travel around the larger particles.

Comparing Figure 9 with Figure 3, it is clear that a low concentration of particles is needed to form two separate rings. The AFM image in Figure 9 shows that only small particles are on the outer edge of the particle ring, which is consistent with Figure 3 and with particle separation. However, two separate rings are not formed because the concentration of particles (0.165 wt % polystyrene) is high and a single thicker ring is formed instead with both particles.

Conclusions

A transport model of an evaporating droplet and two different sized particles was solved and compared to experiments with 1 μm and 3 μm polystyrene spheres in an aqueous droplet. The comparison with experiments show that consideration of thermal variation in the droplet is necessary to accurately predict the particle deposition and is especially important to model the separation of two different sized particles. The Marangoni currents in an evaporating droplet keep the particles suspended for most of the evaporation, depositing a majority of the particles at the end of the evaporation when the droplet is very thin.

Acknowledgments

This material is based upon work supported by the National Science Foundation Graduate Research Fellowship under Grant No. DGE-1333468. The authors also thank PolySciences, Inc. for donating the polystyrene particles used in this work.

Literature Cited

1. Widjaja E, Liu NC, Li M, Collins RT, Basaran OA, Harris MT. Dynamics of sessile droplet evaporation: a comparison of the spine and the elliptic mesh generation methods. *Comput Chem Eng*. 2007; 31(3):219–232.
2. Deegan RD, Bakajin O, Dupont TF, Huber G, Nagel SR, Witten TA. Contact line deposits in an evaporating drop. *Phys Rev E*. 2000; 62(1):756–765.
3. Deegan RD, Bakajin O, Dupont TF, Huber G, Nagel SR, Witten TA. Capillary flow as the cause of ring stains from dried liquid drops. *Nature*. 1997;389:827–829.
4. Hu H, Larson RG. Analysis of the effects of Marangoni stresses on the microflow in an evaporating sessile droplet. *Langmuir*. 2005; 21(9):3972–3980.
5. Parisse F, Allain C. Shape changes of colloidal suspension droplets during drying. *J Phys II*. 1996;6(7):1111–1119.
6. Widjaja E, Harris MT. Particle deposition study during sessile drop evaporation. *Am Inst Chem Eng*. 2008;54(9):2250–2260.
7. Popov YO. Evaporative deposition patterns: spatial dimensions of the deposit. *Phys Rev E*. 2005;71(3):036313.
8. Girard F, Antoni M, Sefiane K. On the effect of Marangoni flow on evaporation rates of heated water drops. *Langmuir*. 2008;24(17): 9207–9210.
9. Trantum JR, Baglia ML, Eagleton ZE, Mernaugh RL, Haselton FR. Biosensor design based on Marangoni flow in an evaporating drop. *Lab Chip*. 2014;14(2):315–324.
10. Trantum JR, Eagleton ZE, Patil CA, Tucker-Schwartz JM, Baglia ML, Skala MC, Haselton FR. Cross-sectional tracking of particle motion in evaporating drops: flow fields and interfacial accumulation. *Langmuir*. 2013;29(21):6221–6231.
11. Hu H, Larson RG. Marangoni effect reverses coffee-ring depositions. *J Phys Chem B*. 2006;110(14):7090–7094.
12. Girard F, Antoni M, Faure S, Steinchen A. Evaporation and Marangoni driven convection in small heated water droplets. *Langmuir*. 2006;22(26):11085–11091.
13. Bhardwaj R, Fang X, Attinger D. Pattern formation during the evaporation of a colloidal nanoliter drop: a numerical and experimental study. *New J Phys*. 2009;11(7):075020.
14. Ristenpart W, Kim P, Domingues C, Wan J, Stone H. Influence of substrate conductivity on circulation reversal in evaporating drops. *Phys Rev Lett*. 2007;99(23):234502.
15. Dunn G, Wilson S, Duffy B, David S, Sefiane K. The strong influence of substrate conductivity on droplet evaporation. *J Fluid Mech*. 2009;623:329–351.
16. Xu X, Luo J. Marangoni flow in an evaporating water droplet. *Appl Phys Lett*. 2007;91(12):124102–1–124102–3.
17. Denkov N, Velev O, Kralchevski P, Ivanov I, Yoshimura H, Nagayama K. Mechanism of formation of two-dimensional crystals from latex particles on substrates. *Langmuir*. 1992;8(12):3183–3190.
18. Denkov N, Velev O, Kralchevsky P, Ivanov I, Yoshimura H, Nagayama K. Two-dimensional crystallization. 1993;361:26.
19. Adachi E, Dimitrov AS, Nagayama K. Stripe patterns formed on a glass surface during droplet evaporation. *Langmuir*. 1995;11(4): 1057–1060.
20. Shmuylovich L, Shen AQ, Stone HA. Surface morphology of drying latex films: multiple ring formation. *Langmuir*. 2002;18(9):3441–3445.
21. Erb RM, Son HS, Samanta B, Rotello VM, Yellen BB. Magnetic assembly of colloidal superstructures with multipole symmetry. *Nature*. 2009;457(7232):999–1002.
22. Han W, Byun M, Lin Z. Assembling and positioning latex nanoparticles via controlled evaporative self-assembly. *J Mater Chem*. 2011; 21(42):16968–16972.
23. Huang J, Kim F, Tao AR, Connor S, Yang P. Spontaneous formation of nanoparticle stripe patterns through dewetting. *Nature Mater*. 2005;4(12):896–900.
24. Jung JY, Kwak HY. Separation of microparticles and biological cells inside an evaporating droplet using dielectrophoresis. *Anal Chem*. 2007;79(13):5087–5092.
25. Jung JY, Kim YW, Yoo JY. Behavior of particles in an evaporating didisperse colloid droplet on a hydrophilic surface. *Anal Chem*. 2009;81(19):8256–8259.

26. Wong TS, Chen TH, Shen X, Ho CM. Nanochromatography driven by the coffee ring effect. *Anal Chem*. 2011;83(6):1871–1873.
27. Welty JR, Wicks CE, Rorrer G, Wilson RE. *Fundamentals of Momentum, Heat, and Mass Transfer*. Hoboken, New Jersey: Wiley, 2009.
28. Nieto de Castro CA, Li SFY, Nagashima A, Trengove RD, Wakeham WA. Standard reference data for the thermal conductivity of liquids. *J Phys Chem Ref Data*. 1986;15(3):1073–1086.
29. Felder RM, Rousseau RW. *Elementry Principles of Chemical Processes*, (With CD). Hoboken, New Jersey: Wiley, 2008.
30. White FM. *Fluid Mechanics*, 7th ed. McGraw-Hill, 2011.
31. Perry RH, Green DW, Maloney JO. *Perry's Chemical Engineers' Handbook, Vol. 7*. New York: McGraw-Hill, 2008.
32. Sung PF. Deposits Formed from the Evaporation of Sessile Droplets and the Interaction of Particles with a Liquid. Ph.D. Thesis, Purdue University, 2012.
33. Widjaja E. Deposition of Colloidal Particles During Sessile Drop Evaporation. Ph.D. thesis, Purdue University, 2007.
34. Hu H, Larson RG. Evaporation of a sessile droplet on a substrate. *J Phys Chem B*. 2000;106:1334–1344.
35. Parsa M, Harmand S, Sefiane K, Bigerelle M, Deltombe R. Effect of substrate temperature on pattern formation of nanoparticles from volatile drops. *Langmuir*. 2015;31:3354–3367.

Appendix

The first validation of this code is the convergence. Using biquadratic elements in the finite element method, each Newton's iteration should converge quadratically. In the simulations presented, quadratic convergence was observed. Once the solution reached a convergence of 10^{-5}, the simulation proceeded to the next time step.

Fluid model validation

A more rigorous validation is comparing the transport model used in this work to published analytical models. Deegan [2] correlates dimensionless flux (J) out of the droplet to radial position in the droplet according to Eq. A1

$$J=(1-r^2)^{-\lambda}$$
$$\lambda=(\pi-2\theta)/(2\pi-2\theta) \tag{A1}$$

where θ is the contact angle between the substrate and the droplet. Figure A1 shows the flux from the transport model used for this research compared to the analytical expression for flux from Eq. A1.

In 2002, Hu and Larson [29] adjusted Deegan's flux expression (Eq. A1) to a similar, but slightly different relationship (Eq. A2)

$$J=(1-r^2)^{-\lambda}$$
$$\lambda=0.5-\theta_c/\pi \tag{A2}$$

Figure A1B compares the transport model used in this work to the analytical expression from Hu and Larson (Eq. A2). As seen in the figures, there is good agreement between the presented transport model and the analytical expressions.

Another method of validation is to examine the vector fields in the simulation. A working model with enough elements to properly simulate the evaporation will have regular vector fields, without vectors that cross each other or wiggles. Figure A2 shows the vector field at the top of the evaporating droplet and at the contact line. These two regions were chosen because they are the most likely to have vectors that cross each other.

Particle model validation

To confirm the accuracy of the particle model, the conservation of particle mass is ensured. Figure A3 shows the conservation of particle mass for a droplet evaporation with $Pe = 1$ and $Da = 10$.

To calculate the particle concentration in the droplet fluid Eq. A3 is used

$$M_{\text{drop}}=\int_{\Omega} c_p r|J|d\xi d\eta \tag{A3}$$

When there is low attraction between the substrate surface and the particles, the Damköhler number is set to zero. In this case, all the particles remain suspended in the fluid for the entire evaporation. Figure A4 shows that in this case mass conservation is maintained.

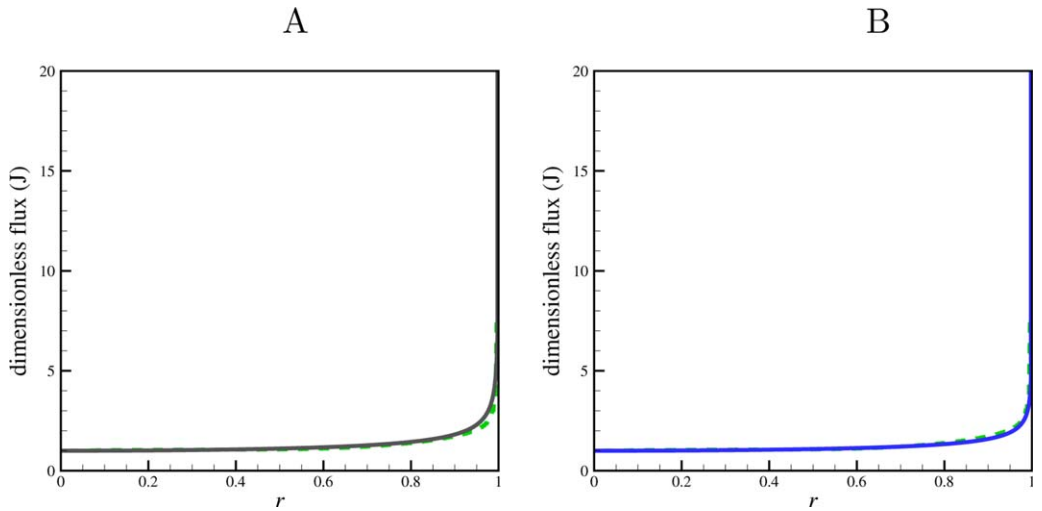

Figure A1. (A) In the solid gray line is the analytical expression for evaporative flux by Deegan et al. (Eq. A1).[2] In the dashed green line is the transport model used in this work. (B) In the solid dark blue line is the analytical expression for evaporative flux by Hu and Larson (Eq. A2).[34]

Again, the green dashed line is the evaporative flux from the transport model used in this work. In both figures *r* is the radial position in the drop, so it is seen that as we approach the contact line, flux from the drop increases significantly. As seen in both the figures, the simulation has excellent agreement with the analytical models. [Color figure can be viewed in the online issue, which is available at wileyonlinelibrary.com.]

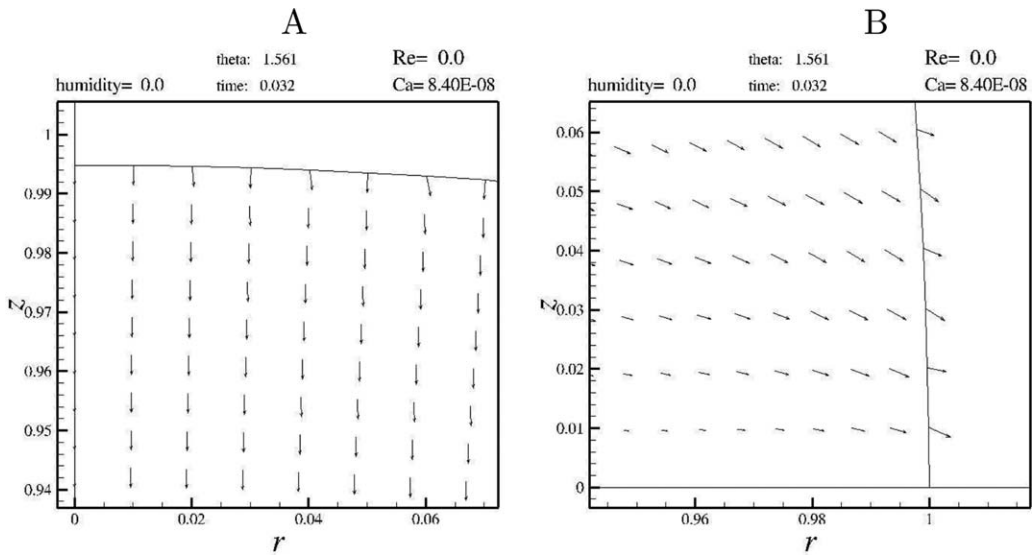

Figure A2. (A) The top of the evaporating droplet at the line of symmetry. (B) The contact line of the same evaporating droplet.

In both images the vectors do not cross each other, an indication of a good model. In this simulation, there is no humidity and the Capillary number, $Ca=8.4\times10^{-8}$.

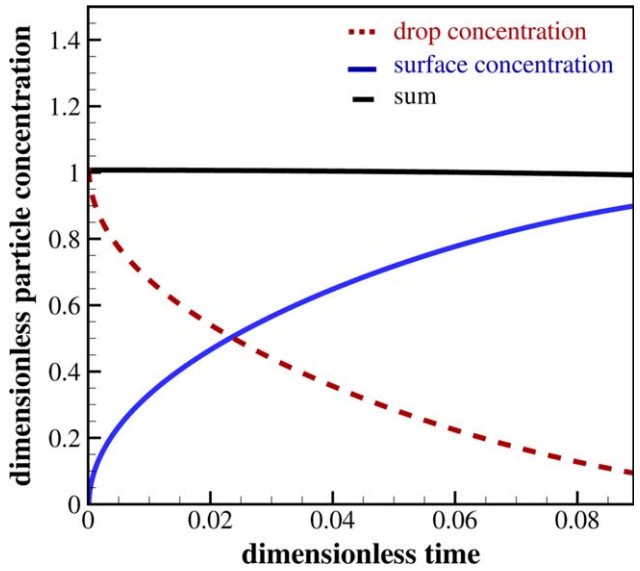

Figure A3. The particles in the evaporating droplet model are conserved.

The solid blue line shows the concentration of particles on the substrate surface. The droplet starts no particles on the surface, then as the droplet evaporates, the particles accumulate on the substrate surface. The dashed red line shows the concentration of particles in the droplet. The concentration of particles on the surface decreases as the particles accumulate on the substrate surface. The dotted black line shows the sum of the particle concentration the droplet fluid and on the substrate surface. This value is constant throughout the evaporation, which validates the particle conservation portion of the model used in this work. This simulation is for a droplet with a radius of 1 mm, a Péclet number of 1, a Damköhler number of 10, a Reynolds number of 6.8×10^{-3} and a Capillary number of 8.4×10^{-7}. [Color figure can be viewed in the online issue, which is available at wileyonlinelibrary.com.]

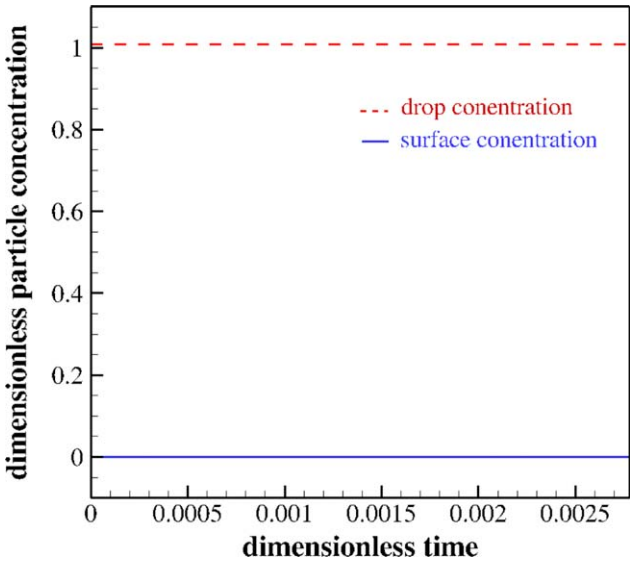

Figure A4. The particles in an evaporating droplet are conserved with $Da = 0$.

The dashed red line is the particle concentration in the fluid, which remains constant. The solid blue line is the particle concentration on the substrate surface, which remains constant at zero. [Color figure can be viewed in the online issue, which is available at wileyonlinelibrary.com.]

Comparison of computational results to experimental results

Finally, the computational results presented in this work were compared with experiments and show good agreement. More detail on this comparison is discussed in the Results Section.

Manuscript received May 28, 2015, and revision received July 13, 2015.